Journal of Material Chemistry A

ARTICLE

On the Chemical Filler-Polymer Interaction of Nano- and Micro-sized ZIF-11 in PBI Mixed Matrix Membranes and their Application for H_2/CO_2 Separation

Received 00th January 20xx,
Accepted 00th January 20xx

DOI: 10.1039/x0xx00000x

www.rsc.org/

Javier Sánchez-Laínez, Beatriz Zornoza*, Carlos Téllez and Joaquín Coronas

The evolution of nano- and micro-sized ZIF-11 (nZIF-11 and ZIF-11, respectively) when embedded into a PBI polymeric matrix is studied. The prepared membranes, with loadings up to 55 wt%, have been characterized through several techniques (XRD, SEM, FTIR, TGA, ^{13}C NMR and XPS) and the changes in the morphology of the fillers upon combination with PBI, as well as in the chemical environment of their main atoms (interactions between the linker of the filler and the benzyl rings of the polymeric bIm units) are discussed. All the membranes have been tested at temperatures ranging between 70 and 200 ^oC to study their H_2/CO_2 separation performance. The integration of both types of MOF in the polymeric phase improves not only the hydrogen permeability but also the selectivity in comparison with the pure polymer in all cases. H_2 permeability increases due to a better diffusion of the penetrants, while CO_2 adsorption on the MOF and solution in the polymer decreases. The best result obtained corresponds to the membrane with 55 wt% loading of ZIF-11, with 495 Barrer of H_2 and a H_2/CO_2 selectivity of 7.0.

Introduction

Gas separation by membrane technology is more efficient than other separation operations such as distillation and absorption processes in terms of both energy cost and separation selectivity. Due to the limitations in the separation performance of polymeric membranes,[1] several solutions have been proposed. Various polymers have been modified with inorganic fillers such as zeolites or mesoporous silicas to produce mixed matrix membranes (MMMs).[2,3]However, it is the embedding of metal organic framework (MOFs) crystals within a polymeric phase and the corresponding gas separation application which has been most extensively studied in recent years.[4-6] Due to the organic linkers present in their structure, MOFs have a better affinity for the polymeric chains than inorganic fillers. The MOF-polymer interface interactions are easier to control in order to avoid non-selective voids between the phases. Furthermore, the selection of the appropriate linkers or the use of post-synthetic functionalization together with the flexibility of MOFs in chemical design and in pore size and shape may facilitate interactions with the polymer and adjust their cavities to a particular application.[7]

Zeoliticimidazolate frameworks (ZIFs) are a subfamily of MOFs in which a metal cation of Zn^{2+} or Co^{2+} is linked to the nitrogen atoms of deprotonated imidazole molecules forming tetrahedral frameworks in zeolite-like topologies.[8] ZIFs constitute highly porous frameworks with extraordinary thermal and chemical stabilities. A striking feature of these materials is that the structure adopted by a given ZIF is determined by link–link interactions rather than by the structure directing agents used in zeolite synthesis.[9] ZIF-11 is especially promising for gas separation owing to its small pore dimensions and to the fact that it can be obtained following several synthesis routes such as solvothermal[10] and non-solvothermal[11] synthesis, sonocrystallization[12] and centrifugal acceleration.[13] It forms a **rho** type zeolitic structure where Zn^{2+} is the metal ion and benzimidazole (bIm) the organic linker.[14] Its well-defined porous structure with large cavities of 1.46 nm connected through pore apertures of 0.3 nm, similar to the kinetic diameter of H_2 (0.29 nm), makes it ideal for hydrogen separation over larger molecules by the sieving process.[10] A H_2/CO_2 selectivity of 262 with a H_2 permeability of 5830 Barrer of ZIF-11 at room temperature has been estimated by molecular simulation, and it is considered a perfect candidate for pre-combustion capture[15]among the different MOFs studied in the literature for CO_2 capture and separation.[16]

Nevertheless, despite all its advantageous properties for gas separation, the micrometric size of ZIF-11 hinders its integration within a polymeric phase when the objective is the formation of thin MMMs. For this reason a nano-sized ZIF-11 (nZIF-11) with an average size of 36±6 nm was successfully synthesized in a previous study. [13] The same chemical composition and thermal stability properties and analogous H_2 and CO_2 adsorption properties as those of the conventional microcrystalline ZIF-11 (i.e. 1.9±0.9 μm) were observed.

The use of polybenzimidazole (PBI) membranes for the separation of H_2/CO_2 mixtures has been widely reported.[17-22] PBI is a polymer

Chemical and EnvironmentalEngineeringDepartment and Instituto de Nanociencia de Aragón (INA)
Universidad de Zaragoza
50018 Zaragoza (Spain)
E-mail: bzornoza@unizar.es

†Electronic Supplementary Information (ESI) available: [TGA and derivative of the different membranes prepared, EDX mapping and stability study in DMAc]. See DOI: 10.1039/x0xx00000x

with high thermal stability, good chemical resistance, impressive compression strength and high intrinsic H_2/CO_2 selectivity. However, its major drawbacks are low permeability and brittleness.[23] Several types of MOFs, such as ZIF-7[18] ZIF-8[24-26] and ZIF-90[27], have been embedded in the PBI continuous phase. MMMs comprising micro-sized ZIF-11 in PBI have hitherto been reported only once, but containing loadings up to 40 wt% and tested at room temperature only.[19]The present work additionally examines membranes containing nano-sized ZIF-11, the use of higher loadings for micro-sized ZIF-11 (up to 55 wt%) and testing at higher temperatures (up to 200 °C). This is of paramount importance for obtaining the best of this high performance polymer. However, ZIF-11 has already shown some lack of chemical stability when exposed to certain experimental conditions.[10] For this reason, it is necessary to explore the evolution of this ZIF in the polymeric matrix in order to ensure that its full properties, suitable for hydrogen separation, are maintained.

In this work nano-sized ZIF-11 (nZIF-11) and micro-sized ZIF-11 have been integrated in a commercial PBI continuous phase in the form of MMMs. The evolution in the morphology of both fillers has been observed by SEM, while changes in chemical bonds at the filler-polymer interphase have been studied by FTIR, NMR and XPS characterization. Furthermore, the crystallinity of the filler inside the polymeric matrix has been checked by XRD analysis. These MMMs, tested at temperatures from 70 to 200 °C, were evaluated for their performance in the separation of H_2/CO_2 mixtures.

Experimental

Chemicals:

Zinc acetate dihydrate ($Zn(CH_3COO)_2 \cdot 2H_2O$), benzimidazole (bIm, $C_7H_6N_2$, 98%), ammonium hydroxide (NH_3, 28–30% aqueous solution), toluene (≥99.5%), and N,N-Dimethylacetamide (DMAc, ≥99.5 %) were purchased from Sigma Aldrich. Methanol (HPLC grade) was purchased from Scharlau. Commercial PBI solution comprising 26 wt% PBI with 1.5 wt% LiCl as stabilizer in DMAc solvent was purchased from PBI performance products.

MOFs synthesis:

The synthesis method of nZIF-11 follows the same procedure used in our previous work.[13] 0.24 g of bIm (2 mmol) was dissolved in 6.4 g of methanol (400 mmol), together with 9.2 g of toluene (100 mmol) and 2.4 g of ammonium hydroxide (40 mmol). 0.22 g of Zinc acetate dihydrate (1 mmol) was dissolved in 3.2 g of methanol (200 mmol). Both solutions were cooled separately to 18 °C and then mixed in a centrifuge flask of 50 mL. The synthesis reaction took place during centrifugation at 10000 rpm for 5 min at that temperature. This procedure prevents the production of large ZIF-11 particles. The solid collected was washed with methanol and centrifuged at 10000 rpm three times for the complete removal of toluene and dried at 100 °C overnight. The molar composition of the mixture was $Zn:bIm:NH_3:CH_3OH:toluene=1:2:40:300:100$.[11]For themicro-sized ZIF-11 synthesis,the same reactant amounts and steps as in the previous procedure were applied. However, instead of centrifuging, the mixture was stirred for 15 min at room temperature before collecting the solid by centrifugation at 10000 rpm and washing it.

MMM preparation:

The required amount of ZIF-11 and nZIF-11 was weighed for each membrane loading, from 10 to 55 wt%, and the corresponding amount of PBI solution was added (previously diluted in DMAc to 15 wt% concentration to avoid problems deriving from viscosity). The resulting solution was further stirred overnight.The casting solution was three times stirred and sonicated alternately for 90 min total time and cast into a petri dish leveled inside an oven at 90 °C. The petri dishes were left uncovered overnight to allow the evaporation of the solvent. After that, the membranes were peeled off from the petri dishes and washed for 8 h in MeOH. Finally, the membranes were treated in a vacuum oven at 130 °C and 10 mbar for 24 h for complete removal of the remaining solvent.

When using nZIF-11 as filler for MMM fabrication, the material was kept in a wet state to minimize agglomeration, i.e. the methanol-collected ZIF-11 nanoparticles were further washed with DMAc. After the second centrifugation, the particles were re-suspended in DMAc prior to use. The suspension concentration was calculated for each membrane loading, 10, 16 and 32 wt%, and the corresponding amount of PBI 15 wt% solution was added. The same procedure was previously used to fabricate MMMs with nZIF-11 and Matrimid®. [13] The membrane thicknesses were tested by a Digimatic Micrometer (measurement range from 0 to 30 mm with an accuracy of ±1 μm). Several equally distributed points (9) on each membrane were measured and the arithmetic mean was taken as the membrane thickness. The MMMs obtained in this work had a thickness of 119±12 μm. For permeation testing of the membranes, circular areas of 15.2 cm^2 were cut from the films.

Characterization of samples:

Powder X-ray diffraction (XRD) spectra of the MOFs and MMMs were acquired using a D-Max Rigaku X-ray diffractometer with a copper anode and a graphite monochromator to select CuKα radiation (λ = 1.540 Å), taking data from 2θ=2.5° to 40° at a scan rate of 0.03 °/s. Thermogravimetric analyses (TGA) were carried out using a Mettler Toledo TGA/STDA 851e. Samples (10 mg) placed in 70 μL alumina pans were heated in air flow from 25 to 900 °C at a heating rate of 10 °C/min. Scanning electron microscopy (SEM) images of the MOFs and membranes were obtained using an Inspect F50 model scanning electron microscope (FEI), operated at 20 kV. Cross-sections of membranes were prepared by freeze-fracturing after immersion in liquid nitrogen and subsequent coating with Pt. Fourier transform infrared spectroscopy (FTIR) was performed on a Bruker Vertex 70 FTIR spectrometer equipped with a DTGS detector and a Golden Gate diamond ATR accessory. Powder samples were prepared by the KBr wafer technique and the measurements were done in a diffuse reflectance module. Both spectra were recorded by averaging 40 scans in the 4000-600 cm^{-1} wavenumber range at a resolution of 4 cm^{-1}. NMR Spectra were recorded in a Bruker Avance III WB400 spectrometer with 4 mm zirconia rotors spun at the magic angle in N_2 at 10 kHz. ^1H-^{13}C CP

spectra were measured using a ^{1}H π/2 pulse length of 3.0 μs, with a contact time (ramp) of 3 ms, a spinal 64 proton decoupling sequence of 5.3 μs pulse length, and a recycle delay of 5 s. 3000 scans were acquired for each spectrum. The chemical shifts were reported relative to TMS. XPS measurements were performed with an Ultra DLD (Kratos Tech.) with Al K_{α}emission (1486.6 eV) operated at 15 kV and 10 mA for the X-ray source. The samples were previously cleaned with an Ar^{+} ion beam, working at 15 kV and 20 mA. The spectra of C 1s and N 1s were recorded and analyzed with Casa XPS software by curve fitting into two or three peaks. All binding energies were corrected for charging of the samples by calibration of the C 1s peak at 284.9 eV. The cross-section of the membranes was also prepared by freeze-fracturing in liquid nitrogen.

Gas separation analysis:

Mixed gas analyses were performed for neat PBI membranes and PBI based MMMs with ZIF-11 and nZIF-11. The membranes were placed in a module consisting of two stainless steel pieces and a 316LSS macroporous disk support (from Mott Co.) with a 20 μm nominal pore size, and gripped inside with Viton O-rings. The permeation module was placed in a UNE 200 Memmert oven to control the temperature of the experiments. Gas separation measurements were carried out by feeding a H_2/CO_2 equimolar mixture (90/90 cm^3(STP)/min) at 330 kPa to the feed side by means of two mass-flow controllers (Alicat Scientific, MC-100CCM-D), while the permeate side of the membrane was swept with a 2 cm^3(STP)/min mass-flow controller stream of Ar at 124 kPa (Alicat Scientific, MC-5CCM-D). Concentrations of H_2 and CO_2 in the outgoing streams were analyzed by an Agilent 3000A online gas microchromatograph equipped with a thermal conductivity detector. Permeability was calculated in Barrer (10^{-10} cm^3(STP)·cm/(cm^2·s·cmHg)) once the steady-state of the exit stream was reached (for at least 3 h), and the separation selectivity was calculated as the ratio of permeabilities.

Results and Discussion

Membrane characterization

Micro- and nano-sized ZIF-11 particles were successfully embedded in the PBI polymeric phase. Fig. 1 shows the cross-sections of the membranes comprising nominal loadings of 10, 16 and 32 wt% of nZIF-11 (actual loadings tested by TGA being 11.0, 15.0 and 30.9 wt%, respectively, as shown in Fig. S1), while those containing 10, 16, 32, 45 and 55 wt% micro-sized ZIF-11 can be seen in Fig. 2 (12.2, 17.0, 31.5, 42.3 and 55.6 wt%, respectively, as shown in Fig. S2). Note that MMMs with higher loadings than 32 wt% were also prepared with nZIF-11 but were broken during handling due to their excessive brittleness. As expected, SEM images revealed a homogeneous dispersion and excellent adhesion of the filler particles within the polymeric phase. However, changes in the morphology of both types of fillers are evident. It can be observed how micro-sized ZIF-11 (Fig. 2a) lost its rhombic dodecahedron form

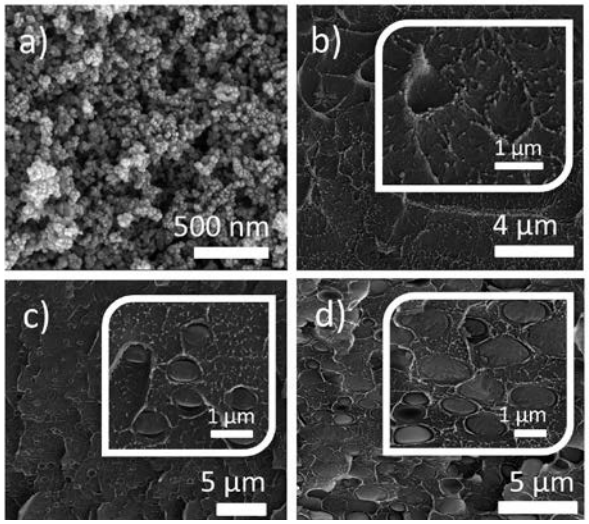

Fig.1. SEM images of a) nZIF-11, and PBI MMMs prepared with nZIF-11 as filler at several loadings: b) 10 wt%, c) 16 wt%, and d) 32 wt%.

of ca. 2.5 μm in size, becoming particles of around 3-4 μm length and 600-800 nm width, thus changing their aspect ratio from 1 to 5.In the case of nZIF-11 (Fig. 1a), the morphology changes are more acute. When embedded in the PBI polymeric phase, this material transformed and grew into lentil-shaped particles whose final size was dependent on the membrane loading (from unappreciable particles revealed by EDX analysis (Figure S3a), ca. 36 nm in size, which cannot be distinguished from the polymer nodules belonging to the PBI matrix at 10 wt% loading (Fig. 1b) to more than 1 μm at 32 wt% loading (Fig. 1d)).Figure S3b shows the EDX-mapping image

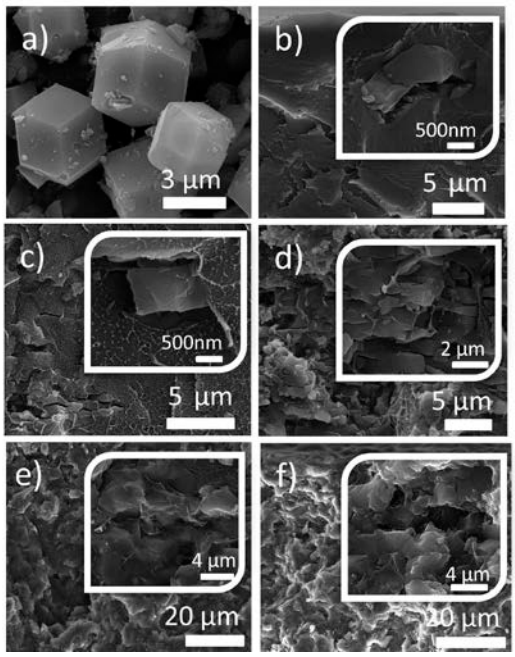

Fig.2. SEM images of a) ZIF-11, and PBI MMMs prepared with ZIF-11 as filler at several loadings: b) 10 wt%, c) 16 wt%, d) 32 wt%, e) 45 wt% and f) 55 wt%.

of the cross-section of the intermediate loading membrane (16 wt%) where the corresponding amount of Zn coming from the MOF can be appreciated.These changes in morphology were probably due to the interaction of the filler with the benzimidazole groups of the polymer, since this behavior was not observed when the material was dispersed in DMAc and dried under the same conditions of the membrane casting (see Fig. S4 and S5). Neither this changes in morphology have been observed when the material was embedded in Matrimid® polyimide,[13]nor when it was ZIF-8 the one embedded in PBI, despite having the same casting conditions.[28]The morphological changes were more significant in the case of the nZIF-11 because of its nano-sized character, and the above mentioned lentil-shape particles appeared of considerably larger size than the initial particles. The evolution of ZIF-8 particles through an Ostwald ripening process has also been reported during the MMM preparation stages.[29]

FTIR spectra of the prepared MMMs and ZIF-11 powder (analogous to nZIF-11) are shown in Fig. 3. Despite the fact that PBI shows very intense bands in the 1300-740 cm^{-1} range,[30,31] the characteristic signals of this MOF can be distinguished. It can be seen that they become more intense as the filler loading increases. The absorbance peak at 1017 cm^{-1} is assigned to the benzene-ring vibration and the signal at 1287 cm^{-1} is related to the imidazole-ring breathing. The peak at 1222 cm^{-1} is caused by the in-plane C-H deformation of the disubstitutedbenzimidazole, while the peak at 902 cm^{-1} is due to the C–H out-of-plane bending of single hydrogen in substituted benzene rings. Finally, the signals at 1180, 1120 and 773 cm^{-1} are due to the benzimidazole in-plane C-H bending, the N-H in-plane bending and the imidazole in-plane ring bending, respectively.[32]

FTIR can assess the chemical environment in the ZIF-11 fillers but not their crystallinity. Fig. 4 shows the XRD spectra of all the membranes containing nZIF-11 and ZIF-11 and the pure PBI film together with the nano- and micro-sized ZIF-11 diffractograms for comparison.

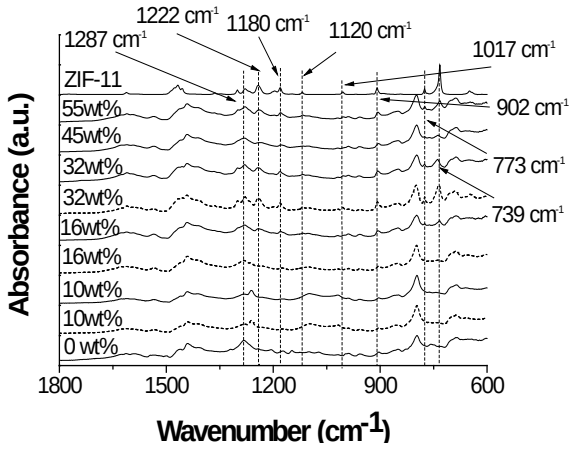

Fig.3. FTIR spectra of the different PBI MMMs prepared with nZIF-11 (dotted line) and ZIF-11 (continuous line) at loadings up to 55 wt% and spectrum of micro-sized ZIF-11.

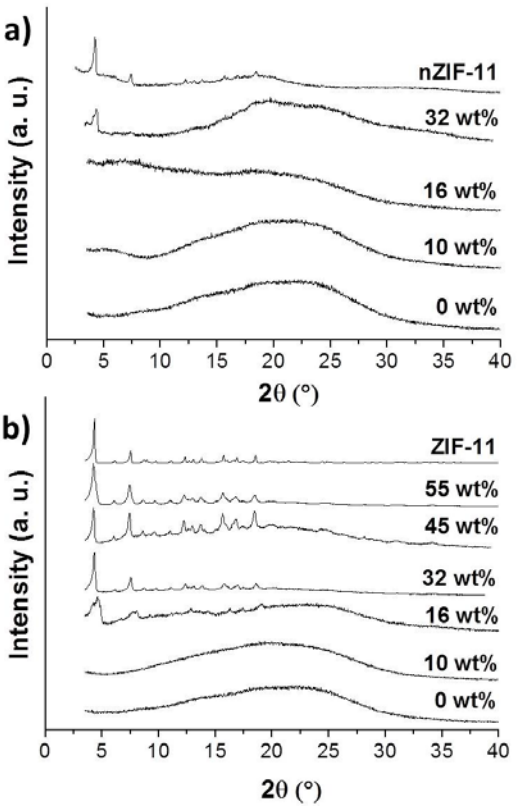

Fig.4. XRD spectra of the different membranes prepared with nZIF-11 (a) and ZIF-11 (b) at loadings up to 55 wt% and spectrum of nano- and micro-sized ZIF-11.

The characteristic peaks of ZIF-11 are only visible athigh loadings (over 16 wt% for ZIF-11 and 32 wt% for nZIF-11 MMMs) because at low loadings the amorphous band of the PBI matrix predominates. As expected, the larger the filler loading, the higher the intensity of these peaks, and the full diffractogram of ZIF-11 is visible at the highest filler loading. In any event, it can be observed how the MMM peaks coincide with those of the filler spectrum, and therefore the crystallinity of the filler remains unaltered when embedded in the polymeric matrix, despite all the morphological changes observed by SEM.The presence of narrow porosity of nZIF-11, a less crystalline material, was also confirmed by H_2 and CO_2 high pressure adsorptionwith uptakes about 50 and 30% lower, for H_2 and CO_2 respectively, than the amounts adsorbed by ZIF-11.[13]

In order to characterize in depth the morphological transformation of both nZIF-11 and ZIF-11 when embedded in PBI polymeric matrix, ^{13}C NMR analyses were performed with bare PBI membrane and MMMs containing both fillers at 32 wt% fixed loading.

The different MMM spectra, as well as those of nZIF-11 and ZIF-11, can be seen in Fig. 5. Six clear peaks can be distinguished in the bare PBI spectrum. The carbon atom between the amino and the imidazole groups (C_1) resonates at 151.9 ppm, while the signals related to the other carbons (C_2-C_7) of the benzimidazole group resonate at 143.1, 134.6, 119.9 and 110.6 ppm. The signals are relatively broad, suggesting both consistent ^1H–^{13}C dipolar couplings and distributions of slightly different chemical environments, due to the packing of the polymer chains.[33] The peak at 129.3 ppm is attributed to aromatic carbons bearing a proton (C_9, C_{10}, and C_{11}). Finally,the signal related to the carbon in the 8 position is located at 134.6 ppm, on the basis of previous liquid NMR studies.[34]

Only four peaks can be distinguished in the spectra of the ZIF-11 and nZIF-11 fillers: at 115.9, 122.5, 141.8 and 150.0 ppm. In the case of the micro-sized ZIF-11, this last peak splits into two signals (151.4 and 148.7 ppm), probably due to differences in the chemical environment arising from the two adjacent benzimidazoles,[35] and from a higher crystallinity (for example, cellulose shows peaks at different ppm values in ordered and disordered structures that could be useful to quantify its crystallinity index[36]). When the MOFs are embedded in the polymeric phase, a slight shift of the peaks to lower ppm values can be appreciated (from 0.4 to 1.4 ppm).

The highest shifts are related to C_4 and C_6, both carbons contained in the benzyl group, substituent in the imidazole molecule, which may prove a π-π interaction between the benzyl rings of the polymeric bIm units and the linker of the ZIFs. In the spectra of both MMMs, the PBI signals at 151.9, 143.1, 119.9 and 110.6 ppm are barely noticeable, while the other two at the central part of the spectrum (134.6 and 129.3 ppm) remain unchanged.

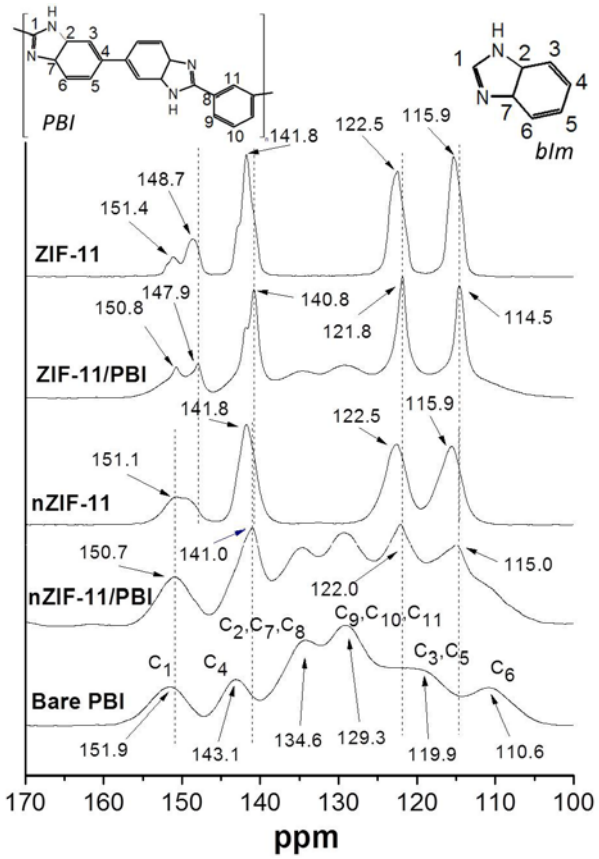

Fig.5. ^{13}C NMR spectra of bare PBI, 32 wt% loading of nZIF-11 and ZIF-11 PBI MMMs and their corresponding fillers.

Note that the signal at 150.7 ppm does not split in the case of the nZIF-11 MMM, suggesting that the material has not changed to a more crystalline phase (ZIF-11) during the membrane formation, which is consistent with the XRD results. Besides, the polymer spectrum dominates over that of the ZIF in this membrane, while it is the filler which dominates in the other MMM containing micro-sized ZIF-11.

The chemical states of nitrogen and carbon in the materials were also characterized by XPS. Recently, a similar study was carried out by Japip*et al.*, to characterize the surface of ZIF-71/6FDA-Durene MMMs.[37] Fig. 6 shows the N 1s and C 1s core-level spectra of the pure PBI membrane, the MMMs containing nZIF-11 (10 and 32 wt%) and ZIF-11 (32 wt%) and the two ZIF fillers. The deconvolution of N 1s spectra involves two peaks (Fig. 6a), –NH– (binding energy BE 400.5 eV) and –N= (BE 398.7 eV), both of the polybenzimidazole molecule, according to the literature for secondary and tertiary amine, respectively.[38] Common XPS features in the nZIF-11 and ZIF-11 suggest that in both samples the chemical environment of nitrogen is similar.

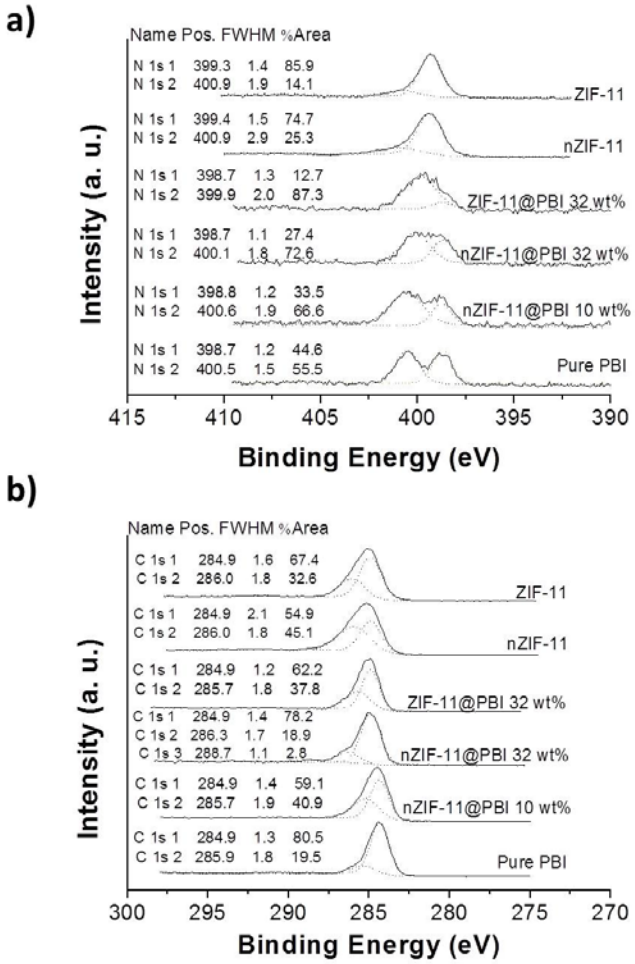

Fig.6. XPS N 1s (a) and C 1s (b) signals of the cross-section of PBI based MMMs and of the corresponding fillers as powder.

However, the peak area ratio of these signals is slightly different. While micro-sized ZIF-11 shows an 85/15 % ratio, in nZIF-11 this ratio is 75/25 %, gaining importance the nitrogen at lower binding energy in the case of ZIF-11 samples, which may be related to its higher degree of crystallinity.[13]

In the case of the membranes' spectra, the pure PBI membrane shows a balanced proportion of both types of nitrogen atom. When embedding both MOFs in the polymeric matrix, this proportion is unbalanced, but unlike the spectra of the powder samples, it is the nitrogen at the higher binding energy which shows a greater peak area ratio. Chemical morphological changes of the filler may be behind this result and might also be indicative of the fact that the MOFs with benzimidazole organic linker are interacting with the PBI polymeric matrix, as appreciated in the NMR spectra. As expected, this imbalance increases with the amount of filler, as can be observed for the nZIF-11 MMMs. For nZIF-11 it can also be appreciated how the proportion between the areas of both types of nitrogen does not reach that of the ZIF-11 MMMs, indicating that the former is not able to crystallize during the membrane formation, as also revealed by NMR. Slight shifts in the signals can be observed for both types of nitrogen when comparing powder with membrane samples suggesting a different chemical environment.

The C 1s spectra for PBI (Fig 6b) show two different signals, C–C (BE 284.9 eV) and C–N (BE 285.9 eV), in accordance with the literature.[39] Note that in the case of PBI containing 32 wt% of nZIF-11 an extra signal appears, referring to the single N=C–N bond of the benzimidazole structure. This group contributes to only 2.8 % of all types of C-containing moieties and therefore it could not have been detected in the other samples, as also occurred with the 8 wt% nZIF-11 MMM. Unlike the N 1s spectra, the proportion in the area of both peaks is quite uneven for the pure polymer sample but becomes more balanced for the fillers, especially for the nZIF-11 sample. Differences between the proportions in both MOFs may again be related to differences in their crystallinity. Besides, the filler loading does not have such a big influence as in the case of N 1s spectra. In the C 1s spectra only the signal of the most energetic carbon slightly shifts, following the same tendency as in the N 1s spectra.

To sum up, the chemical environment provided by the monomeric units of PBI (bIm) is responsible for the changes in the morphology of both nZIF-11 and ZIF-11. There is no clear evidence that new bonds between filler and polymer are created, but there is a clear chemical interaction between both phases. This may be a π-π interaction between the benzyl rings of the polymeric bIm units and the linker of the ZIFs according to NMR results (also verified by XPS analysis). A similar behavior has been previously reported with ZIF-7[40] (same chemical composition as ZIF-11 but with a **sod** structure). This material also changes its form when it gets in contact with DMF at high temperature or with water for a long time, although in this case, the changes also entail a phase transformation.

Permeation performance

Pure PBI membranes and MMMs containing nZIF-11 and ZIF-11 with nominal loadings of 10, 16 and 32 wt% were prepared and tested for comparison. Moreover, micro-sized ZIF-11 membranes were further loaded up to 55 wt%.

Fig. 7a shows the H_2/CO_2 gas separation performance for a 50/50 mixture tested at 150 ºC and 2 bar of driving force. At least 3 MMMs of each loading were fabricated and measured to provide error estimations. The integration of both MOFs in the PBI matrix enhanced the hydrogen permeability, achieving a higher H_2/CO_2 selectivity in comparison with the pure polymer in all cases.

MMMs fabricated with micro-crystalline ZIF-11 showed a similar performance than the analogous nano-sized MOF membranes at the same loading, except for the case of 32 wt% loading where H_2 permeability for the ZIF-11 membrane was about three times higher. As previously reported, nZIF-11, has lower crystallinity than micro-sized ZIF-11,which may lead to poorer separation ability and therefore a worse membrane performance.[13]

However, the more homogeneous distribution of nZIF-11 particles in the PBI phase results in similar performance values to ZIF-11

MMMs at low loadings. Once the membrane loading increases up to 32 wt%, both fillers occupy most of the space of the membrane cross-section leaving enough polymer to cover the particles efficiently. At this point, when both types of MOF are equally dispersed, crystallinity and microporosity start playing a more important role in the separation performance, leading to an enhancement of H_2 permeability for ZIF-11 MMMs. Loadings of 45 and 55 wt% produced membranes with a very little amount of polymer among the particles whose morphology and particle size were modified during the casting procedure (see SEM images in Fig. 2e and Fig. 2f). The gas separation is dominated by the MOF features providing the best membrane performances.

In addition to the previous testing at 150 ºC, MMMs at 45 and 55 wt% loadings of ZIF-11 were also tested at 180-200 ºC so as to improve the membrane performance, and at 70 ºC to complete the study of the temperature influence. All the membranes tested at different temperatures are plotted in Fig. 7b. Note that PBI has an extraordinarily high thermal stability (Fig. S1-S2) with a glass transition temperature of about 426 ºC.[41] Raising the temperature has a beneficial effect on the separation performance, surpassing the Robeson upper bound[1] beyond 32 wt% ZIF-11 loading. The permeability increased at higher temperatures because of the better diffusion of the penetrants while CO_2 adsorption on the MOF and solution in the polymer decreased.

Almost all the membranes show the highest selectivities at the lowest temperature (70 ºC). This tendency has already been reported for PBI MMMs containing ZIF-7 and is due to the balance between the diffusivity selectivity and solubility selectivity for the H_2/CO_2 mixture.[18] At low temperatures the solubility selectivity increases while the diffusivity selectivity decreases. The augmentation of S_{H2}/S_{CO2} exceeds the reduction of D_{H2}/D_{CO2} and therefore the selectivity becomes higher.

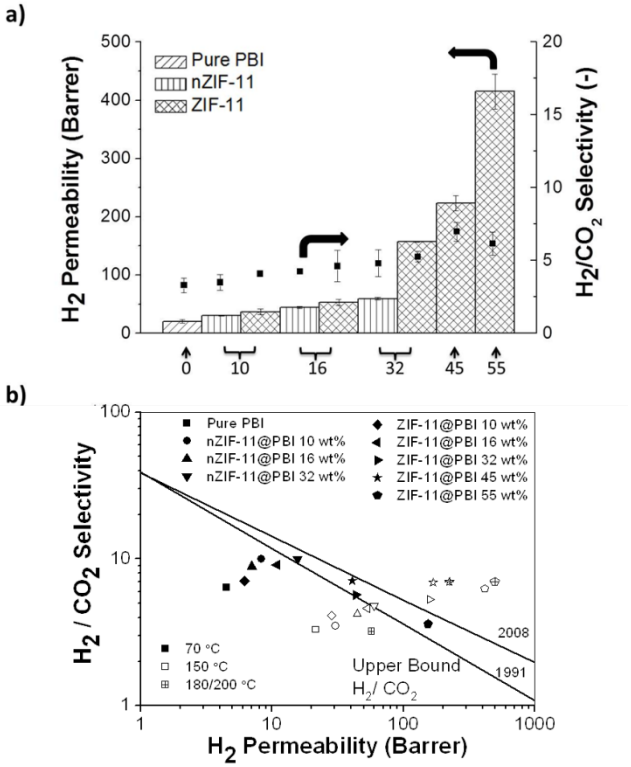

Fig.7. H_2/CO_2 gas separation performance of PBI MMMs containing nZIF-11 and ZIF-11: a) at 150ºC, and b) as a function of the temperature (70 ºC filled, 150ºC empty and 180/200ºC crossed). Robeson´s upper bounds[1] are plotted for comparison.

All the membranes showed permeabilities at least four times higher at 150 ºC than at 70 ºC. The best result obtained with 55 wt% loading of ZIF-11 corresponds to 495 Barrer of H_2 with a H_2/CO_2 selectivity of 7.0, tested at 180 ºC. These results are also in good agreement with the single published paper reporting MMMs with micro-sized ZIF-11 and PBI.[19] In this case the membranes were only tested at 35 ºC and permeability improved when increasing the loading (17.2 Barrer of H_2 for pure polymer membrane to 67.8 Barrer for 16.1 wt% loading and 133.1 Barrer for 29.7 wt%). However, the selectivity barely improved or even decreased over the pure polymer (5.0 for pure PBI, 5.6 for 16.1 wt% loading and 3.7 for 29.7 wt%).

Additionally, in order to estimate the intrinsic properties of the fillers, the Maxwell-Wagner-Sillarequation[42] was applied using the performance results at 150 ºC (see tables S1 and S2). nZIF-11 showed an average H_2 permeability of 4498 Barrer and a H_2/CO_2 selectivity of 64; while ZIF-11, of 9078 Barrer and 104, respectively.

Conclusions

MMMs based on PBI containing nano- and micro-sized ZIF-11 (nZIF-11 and ZIF-11, respectively) as fillers have been successfully

prepared at loadings up to 55 wt%. A chemical morphology transformation for both materials was evident when embedded in the polymeric phase, but were especially acute in the case of the nZIF-11 because of its nano-sized character. While the ZIF-11 lost itsrhombic dodecahedron form becoming particles with higher aspect ratio, those of the nZIF-11 grew and their final size was dependent on the membrane loading. These changes were attributed to the interaction of the filler with the benzimidazole groups of the polymer since this behavior was not observed when the material was dispersed in DMAc and dried under the same conditions of the membrane casting. Despite all these chemical morphological changes, the crystallinity of the fillers remained unaltered according to XRD analysis. Furthermore, π-π interactions between the fillers and the polymer were depicted by NMR analysis, while XPS spectra showed changes in the state of the N and C bonds in the fillers and membranes.

The integration of both MOFs into the PBI polymer phase enhanced in all cases both the H_2 permeability and the selectivity in comparison with the pure polymer in the separation ofH_2/CO_2 at 70-200 ^oC. Besides, MMMs fabricated with micro-crystalline ZIF-11 showed a similar performance to the analogous nano-sized MOF membranes at low loadings (up to 16 wt%). As expected, the permeability increased at higher temperatures due to a better diffusion of the penetrants, while CO_2 adsorption on the MOF and solution in the polymer decreased. The best result of this work corresponded to 495 Barrer of H_2 with a H_2/CO_2 selectivity of 7.0 for the PBI MMM containing 55 wt% of ZIF-11.

Acknowledgements

The research leading to these results has received funding from the European Union Seventh Framework Programme (FP7/2007-2013) under grant agreement n° 608490, project M4CO2. In addition, financial support from the Spanish MINECO (MAT2013-40556-R), the Aragón Government and the ESF is gratefully acknowledged. All the microscopy work was done in the Laboratorio de MicroscopíasAvanzadas at the Instituto de Nanociencia de Aragón (LMA-INA). We thank Dr. Guillermo Antorrena for our fruitful discussions on XPS. Finally, the authors would like to acknowledge the use of Servicio General de Apoyo a la Investigación-SAI, Universidad de Zaragoza.

Notes and references

1 L. M. Robeson, *J. Membr. Sci.,* 2008, **320,** 390-400.
2 B. Zornoza, S. Irusta, C. Téllez and J. Coronas, *Langmuir,* 2009, **25,** 5903-5909.
3 R. Mahajan, R. Burns, M. Schaeffer and W. J. Koros, *J. Appl. Polym. Sci.,* 2002, **86,** 881-890.
4 H. B. T. Jeazet, C. Staudt and C. Janiak, *Dalton Trans.,* 2012, **41,** 14003-14027.
5 T. Rodenas, M. van Dalen, E. García-Pérez, P. Serra-Crespo, B. Zornoza, F. Kapteijn and J. Gascon, *Adv. Funct. Mater.,* 2014, **24,** 249-256.
6 A. Sabetghadam, B. Seoane, D. Keskin, N. Duim, T. Rodenas, S. Shahid, S. Sorribas, C. L. Guillouzer, G. Clet and C. Tellez, *Adv. Funct. Mater.,* 2016, .
7 B. Zornoza, C. Tellez, J. Coronas, J. Gascon and F. Kapteijn, *Microporous Mesoporous Mater.,* 2013, **166,** 67-78.
8 Y. Lee, J. Kim and W. Ahn, *Korean J. Chem. Eng.,* 2013, **30,** 1667-1680.
9 H. Hayashi, A. P. Cote, H. Furukawa, M. O'Keeffe and O. M. Yaghi, *Nat. Mater.,* 2007, **6,** 501-506.
10 K. S. Park, Z. N. Ni, A. P. Coˆ te, J. Y. Choi, R. Huang, F. J. Uribe-Romo, H. K. Chae, M. O'Keeffe and O. M. Yaghi, *PNAS,* 2006, **103,** 10186-10191.
11 M. He, J. Yao, Q. Liu, Z. Zhongb and H. Wang, *Dalton Trans.,* 2013, **42,** 16608-16608–16613.
12 B. Seoane, J. M. Zamaro, C. Tellez and J. Coronas, *CrystEngComm,* 2012, **14,** 3103-3107.
13 J. Sánchez-Laínez, B. Zornoza, Á. Mayoral, Á. Berenguer-Murcia, D. Cazorla-Amorós, C. Téllez and J. Coronas, *J. Mater. Chem. A,,* 2015, .
14 J. C. Tan, T. D. Bennett and A. K. Cheetham, *Proc. Natl. Acad. Sci. U. S. A.,* 2010, **107,** 9938-9943.
15 A. W. Thornton, D. Dubbeldam, M. S. Liu, B. P. Ladewig, A. J. Hilla and M. R. Hill, *Energy Environ. Sci.,* 2012, **5,** 7637–7646.
16 Z. Zhang, Z. Yao, S. Xiang and B. Chen, *Energy Environ. Sci.,* 2014, **7,** 2868-2899.
17 S. Choi, J. Coronas, E. Jordan, W. Oh, S. Nair, F. Onorato, D. F. Shantz and M. Tsapatsis, *Angew. Chem. Int. Ed.,* 2008, **47,** 552-555.
18 T. Yang, Y. Xiao and T.S. Chung, *Energy Environ. Sci.,* 2011, **4,** 4171-4180.
19 L. Li, Y. Jianfeng, X. Wang, Y. Chen and H. Wang, *J. Appl. Polym. Sci.,* 2014, **131,** 41056.
20 X. Li, R. P. Singh, K. W. Dudeck, K. A. Berchtold and B. C. Benicewicz, *J. Membr. Sci.,* 2014, **461,** 59-68.
21 S. Kumbharkar, Y. Liu and K. Li, *J. Membr. Sci.,* 2011, **375,** 231-240.
22 B. P. Biswal, A. Bhaskar, R. Banerjee and U. K. Kharul, *Nanoscale,* 2015, **7,** 7291-7298.
23 T.S. Chung, *J. Macromol. Sci., Part C: Polymer Reviews,* 1997, **37,** 277-301.
24 T. Yang, G. M. Shi and T.S. Chung, *Adv. Energy Mater.,* 2012, **2,** 1358-1367.
25 T. Yang and T. S. Chung, *Int. J. Hydrogen Energy,* 2013, **38,** 229-239.
26 A. Bhaskar, R. Banerjee and U. Kharul, *Journal of Materials Chemistry A,* 2014, **2,** 12962-12967.
27 T. Yang and T.S. Chung, *J. Mater. Chem. A,* 2013, **1,** 6081-6090.
28 J. Sanchez-Lainez, B. Zornoza, S. Friebe, J. Caro, S. Cao, A. Sabetghadam, B. Seoane, J. Gascon, F. Kapteijn, C. Guillouzer, G. Clet, M. Daturi, C. Tellez, J. Coronas,*J. Membr. Sci.,***2016**. http://dx.doi.org/10.1016/j.memsci.2016.05.039.
29 J. A. Thompson, K. W. Chapman, W. J. Koros, C. W. Jones and S. Nair, *Microporous Mesoporous Mater.,* 2012, **158,** 292-299.
30 P. Musto, F. Karasz and W. MacKnight, *Polymer,* 1993, **34,** 2934-2945.
31 P. Christensen and S. Jones, *Polym. Degrad. Stab.,* 2014, **105,** 211-217.
32 D. P. Drolet, D. M. Manuta, A. J. Lees, A. Katnani and G. J. Coyle, *Inorg. Chim. Acta,* 1988, **146,** 173-180.

33 A. S. Cattaneo, D. C. Villa, S. Angioni, C. Ferrara, E. Quartarone and P. Mustarelli, *J. Phys. Chem C,* 2015, **119,** 18935-18944.
34 J. Grobelny, D. M. Rice, F. E. Karasz and W. J. MacKnight, *Macromolecules,* 1990, **23,** 2139-2144.
35 S. Zhu, L. Yan, D. Zhang and Q. Feng, *Polymer,* 2011, **52,** 881-892.
36 S. Park, J. O. Baker, M. E. Himmel, P. A. Parilla and D. K. Johnson, *Biotechnol. Biofuels,* 2010, **3,** 1.
37 S. Japip, K. Liao, Y. Xiao and T.S. Chung, *J. Membr. Sci.,* 2016, **497,** 248-258.
38 D. W. Mangindaan, N. M. Woon, G. M. Shi and T. S. Chung, *Chem. Eng. Sci.,* 2015, **122,** 14-23.
39 D. Mangindaan, W. Kuo, C. Chang, S. Wang, H. Liu and M. Wang, *Surf. Coat. Technol,* 2011, **206,** 1299-1306.
40 P. Zhao, G. I. Lampronti, G. O. Lloyd, M. T. Wharmby, S. Facq, A. K. Cheetham and S. A. Redfern, *Chem. Mater.,* 2014, **26,** 1767-1769.
41 S. S. Hosseini and T. S. Chung, *J. Membr. Sci.,* 2009, **328,** 174-185.
42 R. Bouma, A. Checchetti, G. Chidichimo and E. Drioli, *J. Membr. Sci.,* 1997, **128,** 141-149.